Development 137, 4091-4099 (2010) doi:10.1242/dev.057455

When whorls collide: the development of hair patterns in frizzled 6 mutant mice

Yanshu Wang[1,4], Hao Chang[1,4] and Jeremy Nathans[1,2,3,4,*]

SUMMARY

Surface appendages such as bristles, feathers and hairs exhibit both long- and short-range order. In the frizzled 6 null (*Fz6*$^{-/-}$) mouse the orientations of the earliest born hair follicles are uncorrelated, but over time the follicles reorient to create patterns that are characterized by a high degree of local order. By quantifying follicle orientations over time, in both living and fixed tissues, we define the time course of local hair follicle refinement and the resulting evolution of a montage of competing patterns in *Fz6*$^{-/-}$ skin. We observe an apparently local process that within one week can organize a field of many tens of thousands of follicles, generating long-range order that extends over distances of more than one centimeter. Physical systems that undergo an analogous ordering of vector components suggest potential mechanisms that might apply to the patterning of hair follicles and related biological structures.

KEY WORDS: Frizzled 6, Hair pattern, Planar cell polarity, Mouse

INTRODUCTION

Macroscopic patterns based on the locations, sizes, shapes and orientations of surface structures are ubiquitous in the animal kingdom. Examples of patterned surface structures include cuticular plates and bristles in invertebrates, and feathers, hairs, scales and dermatoglyphs (fingerprints) in vertebrates. For structures that are densely distributed over the body surface, there is generally a precise relationship between the orientations of the structures and the body axes, as well as a correlation between the orientations of adjacent structures. The phenomenon of spatial order within a two-dimensional array of biological structures is referred to as tissue or planar cell polarity (PCP).

The developmental mechanisms responsible for generating surface order have been an object of study for more than half a century. Classic experiments in which a small region of insect cuticle was rotated revealed a response that minimizes the local discontinuity in bristle orientation by rotating nearby bristles (Wigglesworth, 1940; Locke, 1959; Lawrence, 1966). More recently, genetic analyses in *Drosophila* have revealed two signaling systems – one mediated by the *fat* (*ft*) and *dachsous* (*ds*) genes, and the second mediated by the *frizzled* (*fz*), *starry night* [*stan*; also known as *flamingo* (*fmi*)] and *Van Gogh* (*Vang*) genes – that control the orientation of cuticular structures (Lawrence et al., 2007; Simons and Mlodzik, 2008; Axelrod, 2009). Homologs of these genes are present in vertebrates and are required for a wide variety of polarized morphological processes, including axon guidance in the brain and spinal cord, neural tube closure, motoneuron migration in the hindbrain, and the orientation of inner ear sensory neurons, motile cilia, hair follicles and cell division axes (Kibar et al., 2001; Murdoch et al., 2001; Wang et al., 2002; Wang et al., 2006a; Wang et al., 2006b; Wang et al., 2006c; Curtin et al., 2003; Lyuksyutova et al., 2003; Montcouquiol et al., 2003; Guo et al., 2004; Tissir et al., 2005; Saburi et al., 2008; Zhou et al., 2008; Qu et al., 2010; Song et al., 2010; Tissir et al., 2010).

In mammals, null mutations in frizzled 6 (*Fz6*, *Fzd6*) or *Celsr1* (a *stan* homolog) produce a phenotype in utero of hair follicle orientations that appear to be randomized (Wang et al., 2006a; Ravni et al., 2009). However, during the first postnatal week, the follicles reorient, resulting in the development of large-scale patterns (Guo et al., 2004; Wang et al., 2006a; Ravni et al., 2009). During the same time window, an analogous, but more subtle, reorientation of follicles occurs in wild-type (WT) mice, leading to greater uniformity in follicle orientations (Wang et al., 2006a). These observations imply the existence of two temporally and mechanistically distinct follicle alignment processes. The first process acts early, is dependent on *Fz6* and *Celsr1*, and in the WT produces a field in which the follicle vectors are roughly aligned to the body axes. The second process acts later, is independent of *Fz6* and *Celsr1*, and refines follicle orientations in a manner that minimizes local differences in orientation. The second process appears to be the mammalian analog of the bristle realignment program revealed by the insect cuticle rotation experiments noted above.

The present paper focuses on the spatial and temporal dynamics of the hair follicle reorientation process. Our analysis of follicle orientations in *Fz6*$^{-/-}$ mice during late gestation and the first postnatal week, in both living and fixed tissues, reveals an apparently local alignment process that generates macroscopic patterns de novo. These patterns compete with each other, expand over time, and eventually generate long-range order over distances of more than one centimeter.

MATERIALS AND METHODS

Mouse lines and husbandry

The *Fz6*$^{-/-}$, *Vangl2*$^{Lp/+}$ and *K17-GFP* lines were maintained and genotyped as previously described (Wang et al., 2006a; Wang et al., 2006b).

Preparation and imaging of mouse skin flat mounts

To visualize follicles using *K17-GFP* (before P0), skins were dissected and fixed as described below for postnatal skins, and then imaged on a Zeiss 510 confocal microscope. To visualize follicles using the endogenous

[1]Department of Molecular Biology and Genetics, [2]Department of Neuroscience, [3]Department of Ophthalmology and the [4]Howard Hughes Medical Institute, Johns Hopkins University School of Medicine, Baltimore, Maryland 21205, USA.

*Author for correspondence (jnathans@jhmi.edu)

Accepted 29 September 2010

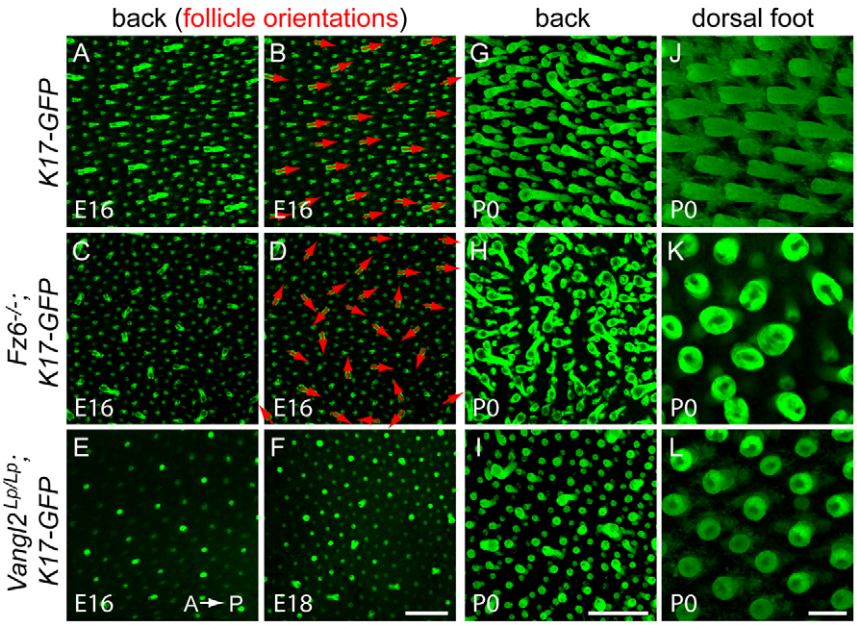

Fig. 1. Hair follicle orientations on the back and on the dorsal surface of the feet in late embryonic and neonatal wild-type, *Fz6*$^{-/-}$ and *Vangl2*$^{Lp/Lp}$ mice. Follicles in *z*-stacked confocal images of skin flat-mounts are visualized by the fluorescence of a *K17-GFP* transgene (green). (**A-I**) Images of back skin are oriented with anterior to the left and posterior to the right, as indicated in E. Red arrows in B and D indicate follicle orientations for the guard hairs in the wild-type (WT) and *Fz6*$^{-/-}$ images A and C. (**J-L**) Images of dorsal foot skin are oriented with proximal to the left and distal to the right. Scale bars: 400 μm in A-I; 100 μm in J-L.

melanin pigment (after P0), the dorsal skin was dissected free of underlying connective tissue, flattened by fixing its cut edges to a flat Sylguard surface with insect pins, fixed overnight in 4% paraformaldehyde in PBS, dehydrated through a graded alcohol series, and then transferred to a glass dish for clarification in benzyl benzoate:benzyl alcohol (BBBA). For long-term storage, skins were placed in ethanol at –20°C. Two imaging methods were used. Low-resolution images were obtained by scanning each BBBA-clarified skin on a flatbed scanner at 12,800 dpi. Although flatbed scanning can produce high-resolution images of thin objects, such as photographic negatives, this method produces images of mouse skin with a resolution that is only about half the diameter of a hair follicle. Higher resolution images were obtained with a Zeiss dissecting microscope. For each skin, a montage of the head and back was manually assembled from ~30 grayscale images.

Imaging hair follicles in living mice

Early postnatal mice were immobilized without anesthesia by placing them ventral side down on a Petri plate and taping three limbs to the surface. The fourth limb was taped to a gently sloping wedge (to compensate for the proximal-to-distal narrowing of the paw), and covered with glycerol to clarify the superficial layers of skin and convert the optically rough surface into a relatively smooth glycerol-air interface. Images were collected on a Zeiss fluorescence dissecting microscope, and the follicle angles were scored by manually adjusting overlaid arrows in Adobe Photoshop.

Measuring interfollicle angular differences

Sixty-three evenly spaced vectors arranged in a rectilinear 6×9 grid (encompassing an area of 2×2.5 mm) were overlaid on each flat-mount skin image in Adobe Illustrator. The 6×9 grid spacing closely approximates the spatial density of the subset of most mature follicles for which the orientations can be scored at P0. Each vector was then moved to the location of the closest scorable follicle and manually rotated to match the orientation of the shaft of that follicle. To maintain a constant spatial scale of vector comparisons across skin samples, the same 6×9 grid was used to score skin images across all ages examined, even though (1) the number of mature follicles rapidly increases with age so that for progressively older skins the 63 vectors sample a progressively smaller fraction of the scorable follicles within the grid area, and (2) the early postnatal mice are growing rapidly so that the constant grid size represents a progressively smaller fraction of the body surface area with age. For each grid of 63 vectors, the angular differences between all pairs of nearest-neighbor vectors were calculated.

Visualizing large-scale hair patterns

A standard, rectilinear 20×44 grid of evenly spaced vectors was overlaid on the skin montage and each vector was manually rotated to match the orientations of the follicles in its immediate neighborhood. Singularities (crosses or whorls) were scored by visual inspection.

RESULTS

Local refinement of hair follicle orientations in early postnatal development

Previous work identified multiple phenotypes in mouse embryos homozygous for the *Looptail* (*Lp*) allele of the PCP gene van gogh-like 2 (*Vangl2*), including an open neural tube and misorientation of inner ear sensory neurons. To visualize and compare hair follicle phenotypes in late gestation WT, *Fz6*$^{-/-}$ and *Vangl2*$^{Lp/Lp}$ fetuses, we used a keratin 17-*green fluorescent protein* (*K17-GFP*) transgene to visualize follicle orientations in flat-mounts of skin between embryonic day (E) 16 and E18 (Fig. 1A-F). We observed a sparse population of early developing guard hair follicles on the back that have roughly parallel orientations in WT fetuses, uncorrelated orientations in *Fz6*$^{-/-}$ fetuses, and orientations that are roughly perpendicular to the skin surface in *Vangl2*$^{Lp/Lp}$ fetuses. These observations are consistent with previous analyses of transverse sections through *Vangl2*$^{Lp/Lp}$ skin (Devenport and Fuchs, 2008); the same study also reported perpendicularly oriented prenatal follicles in mice homozygous for the *Crsh* allele of *Celsr1*. The distinctive patterns of WT, *Fz6*$^{-/-}$ and *Vangl2*$^{Lp/Lp}$ follicle orientations were seen at postnatal day (P) 0 on the back and on the dorsal surface of the feet (Fig. 1G-L). The failure of *Vangl2*$^{Lp/Lp}$ follicles to orient within the plane of the skin does not appear to be a consequence of the mild growth retardation that characterizes these fetuses, as *Vangl2*$^{Lp/Lp}$ follicles at E18 and P0, which are similar in size to WT and *Fz6*$^{-/-}$ follicles at E16, remained oriented perpendicular to the skin surface (compare Fig. 1A,C,F,I).

These observations suggest that there are at least two different classes or severities of follicle misorientation associated with defects in PCP signaling: follicle orientations that are (1) uncorrelated and oblique to the skin surface (*Fz6*$^{-/-}$ and *Celsr1*$^{-/-}$) (Ravni et al., 2009) or (2) vertically oriented (*Celsr1*$^{crsh/crsh}$ and *Vangl2*$^{Lp/Lp}$). If we suppose that the *Celsr1*^{crsh} and *Vangl2*^{Lp}

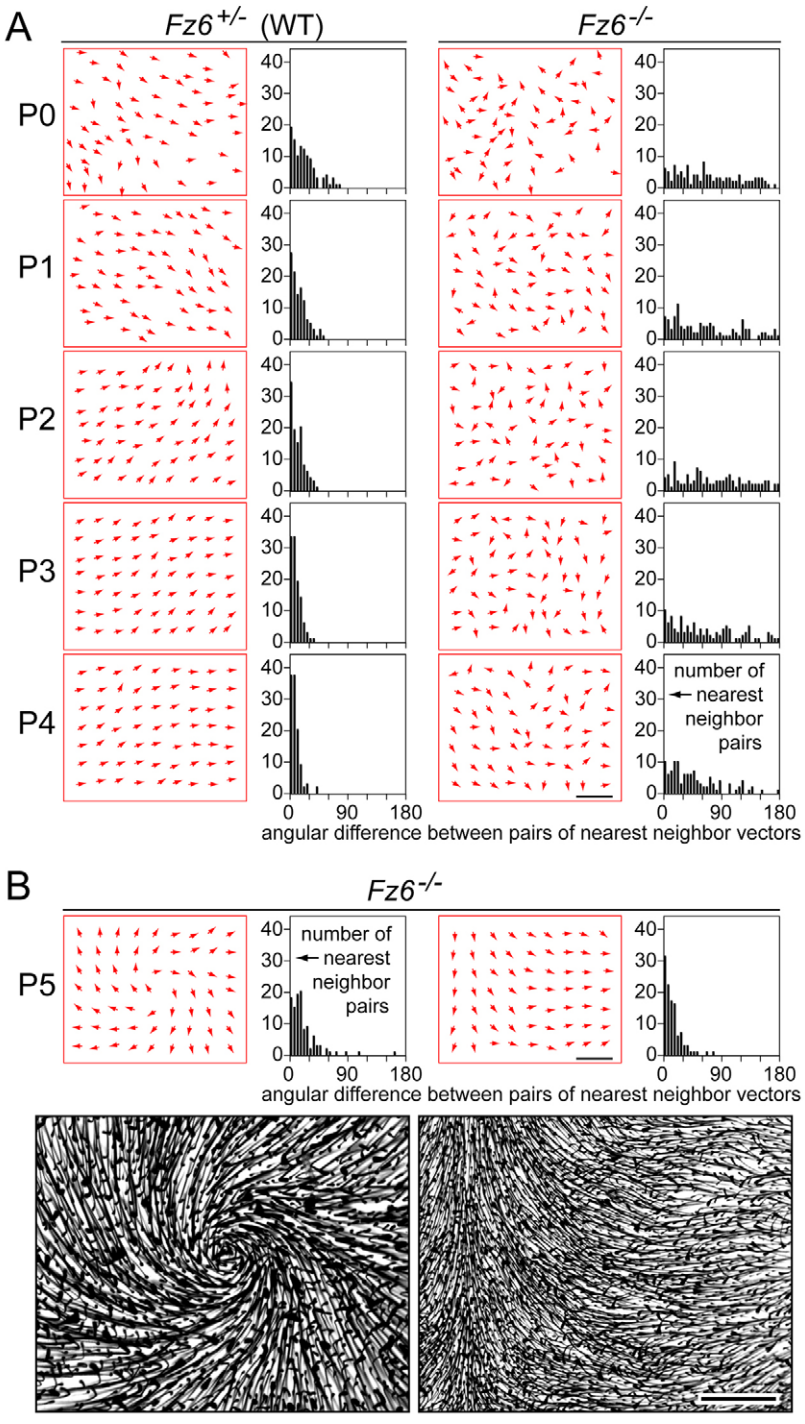

Fig. 2. Progressive decrease in orientation differences between neighboring follicles in postnatal *Fz6*$^{+/-}$ (WT) and *Fz6*$^{-/-}$ mouse back skin. (**A**) At the indicated ages, 2.0 mm×2.5 mm regions were scored for the orientations of a sample of 63 follicles that were closest to the points of a 7×9 grid. For each image, the vector map shows the orientations of the shafts of the sampled follicles. For each vector map, the difference in orientation between each sampled follicle and the four sampled follicles located immediately above, below, left and right is plotted on the adjacent histograms. Vector maps for P0-P4 skins are oriented with anterior to the left and posterior to the right. (**B**) P5 *Fz6*$^{-/-}$ vector maps (top) and corresponding skin flat-mount images (bottom) are oriented anterior up and posterior down. All vector maps are shown at the same scale. Scale bars: 500 μm.

missense alleles (Kibar et al., 2001; Murdoch et al., 2001; Curtin et al., 2003) confer a more severe phenotype because they code for dominant-negative proteins, then one interpretation of the diversity of follicle orientation phenotypes is that the vertical phenotype corresponds to a complete loss of Fz or Celsr function, whereas the uncorrelated and oblique phenotype corresponds to a partial loss of Fz or Celsr function. If correct, this hypothesis implies partial redundancy of *Fz6* and *Celsr1* with other Fz and Celsr family members, respectively.

In a previous study, we described a progressive refinement of hair follicle orientations during early postnatal development (Wang et al., 2006a), and we inferred, but did not quantify, the age-dependent decrease in the differential orientations of neighboring follicles. In Fig. 2, we quantify this parameter. At daily intervals, WT and *Fz6*$^{-/-}$ back skins were flat mounted, 63 follicles from the center of the back were sampled using the vertices of a 7×9 rectangular grid (encompassing an area of 2.0×2.5 mm), and the follicle orientations measured. The histograms show differences between follicle angles for all pairwise comparisons of adjacent grid points. As shown in Fig. 2A, at younger ages, the follicles that are mature enough to permit an accurate measurement of their orientations are often some distance from the nearest grid points; thus, the distances between scored follicles is more variable at this time point. In Fig. 2B, two regions of *Fz6*$^{-/-}$ skin at P5 are shown

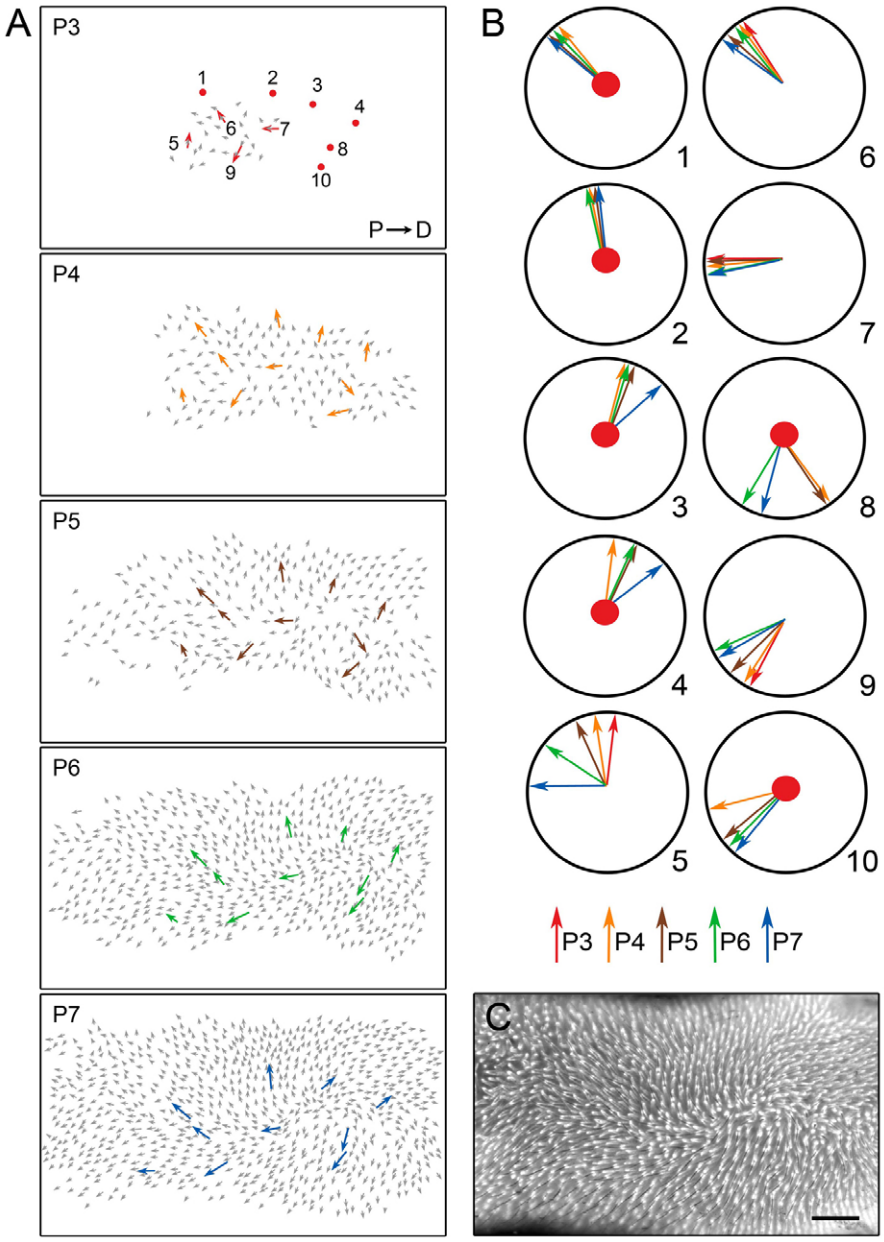

Fig. 3. Live imaging of *Fz6*$^{-/-}$*;K17-GFP* follicles on the mouse dorsal foot between P3 and P7. (**A**) Vector maps with ten representative follicles highlighted and numbered. Proximal (P) is to the left and distal (D) is to the right. (**B**) Polar plot of the orientations of the numbered follicles. Follicles 1-4, 8 and 10 were too immature and/or not sufficiently angled with respect to the skin surface to score at P3; this time point is represented by the central circle on the polar plot. (**C**) Live foot at P7 showing *K17-GFP* fluorescence in follicles. This image corresponds to the adjacent P7 vector map. Scale bar: 500 μm.

to illustrate the degree of nearest-neighbor alignment in regions that are either centered on, or distant from, a whorl (the left and right panels, respectively). Fig. 2 shows that both WT and *Fz6*$^{-/-}$ skin exhibit a progressive narrowing of angular differences between nearby follicles during the first postnatal week.

Live imaging of hair follicle reorientation

Our previous analyses of hair follicle orientation in *Fz6*$^{-/-}$ mice relied on longitudinal comparisons between different mice, with images collected post-mortem from intact mice or dissected skin (Guo et al., 2004; Wang et al., 2006a). Ideally, one would image the same follicles over time in a living mouse. However, live imaging of skin faces a series of technical challenges including: (1) immobilizing the region to be imaged without distorting the skin and (2) imaging inside the skin at optical wavelengths. We have attempted to solve these problems by imaging the feet of unanesthetized postnatal mice. The dorsal surface of the foot appears to be the most favorable site for live imaging of hair follicles because the foot can be secured to a fixed surface so that it is not subject to movement artifacts, and because, in contrast to the skin on the head and torso, the skin on the foot is relatively taut in early postnatal life. We also found that it is possible to simultaneously increase the optical clarity of the skin and create a relatively smooth air-tissue surface by applying a few drops of 100% glycerol, a method that is simple and non-toxic. To improve the visualization of individual follicles we worked with black *Fz6*$^{-/-}$*;K17-GFP* mice, so that each hair shaft is seen as a black line within a fluorescent follicle (Fig. 3C).

Images were collected daily from three *Fz6*$^{-/-}$*;K17-GFP* mice between P3 and P7, and individual follicle orientations were measured and represented as vectors (Fig. 3 and see Figs S1 and S2 in the supplementary material). At P3, only a small minority of follicles is sufficiently mature that their orientations can be reliably scored with the live-imaging protocol outlined above. By contrast, imaging of fixed and dissected *K17-GFP* skin using confocal microscopy permits the orientations of less mature follicles to be

scored (Fig. 1J,K). Fig. 3 shows that between P3 and P7, follicle orientations on the *Fz6*$^{-/-}$ foot change by as much as 90°, with the majority of follicles showing changes between 0 and 45°. For most follicles, changes in orientation over the 4-day period of observation proceeded monotonically (Fig. 3B). By P7, the central whorl on each foot, which is a characteristic of all *Fz6*$^{-/-}$ mice, was readily apparent (Fig. 3A,C).

Follicle bending near the center of a whorl

In previous work, we noted that *Fz6*$^{-/-}$ hair follicles show, on average, more bending than their WT counterparts (Wang et al., 2006a). The bending could arise from a differential mobility of the follicle shaft, which is the region closest to the epidermis, versus the follicle bulb, which is the region furthest from the epidermis. As the invagination point of each follicle at the epidermis appears to be fixed in a regular lattice at the start of follicle development (Sick et al., 2006), any movement of the follicle shaft must consist of a rotation about the point of epidermal insertion. Since the orientation of the hair shaft beyond the skin surface matches the orientation of the follicle shaft rather than that of the follicle bulb, it follows that the reorientation of the shaft is the critical parameter in determining the hair pattern.

Fig. 4 illustrates an extreme example of the differential orientations of follicle bulbs and shafts. For this example, we have chosen a whorl from the P8 *Fz6*$^{-/-}$*;Vangl2*$^{Lp/+}$ back skin shown in Fig. 6 (*Fz6*$^{-/-}$ and *Fz6*$^{-/-}$*;Vangl2*$^{Lp/+}$ mice show very similar hair patterning phenotypes). Fig. 4A shows the center of a whorl at three focal planes: near the base of the dermis, at the level of the follicle bulbs; in the center of the dermis, at the midpoint of the follicle shafts; and at the epidermal surface, where the hair emerges from the skin. For a subset of follicles in the images reproduced on the right-hand side of Fig. 4A, the orientations of the bulb and the shaft are delineated by red and green arrows, respectively. It is apparent that many follicles near the center of the whorl have a very pronounced bend. A sample of 60 follicles near the center of the whorl had an average bulb versus shaft difference of ~140° (Fig. 4B). By contrast, for a sample of 60 follicles far from the whorl, the average bulb versus shaft difference was ~20°. We note that if each *Fz6*$^{-/-}$ follicle were to reorient by the most efficient path from its initial orientation (which appears to be approximately random) to its final orientation, then the mean rotation would be ~90°, with a range of 0-180°. If the angular difference between bulb and shaft reflects the extent of rotation of each follicle – as would be the case if, for example, the shaft rotated to the full extent required to create the hair pattern while the bulb rotated less – then the comparison in Fig. 4 suggests that follicles near the center of a whorl reorient more than the average follicle. These considerations suggest that the follicles near the center of the whorl in Fig. 4 might have rotated, on average, more than 90°, perhaps because interactions between neighboring follicles produced an ever tighter spiraling of vector orientations towards the center of the whorl.

Large-scale individual-specific hair patterns in *Fz6*$^{-/-}$ mice

A striking feature of the *Fz6*$^{-/-}$ phenotype is the interindividual variability in the hair patterns on the head and back (Guo et al., 2004). To systematically assess this variability, we constructed 'vector maps' of *Fz6*$^{-/-}$ skins between P5 and P8 by aligning the orientations of vectors located at the vertices of a grid, so that each vector matches the average local follicle orientation (Fig. 5). Prior to P5, large variations in the orientations of neighboring follicles make it difficult to assess the average orientation (Fig. 2).

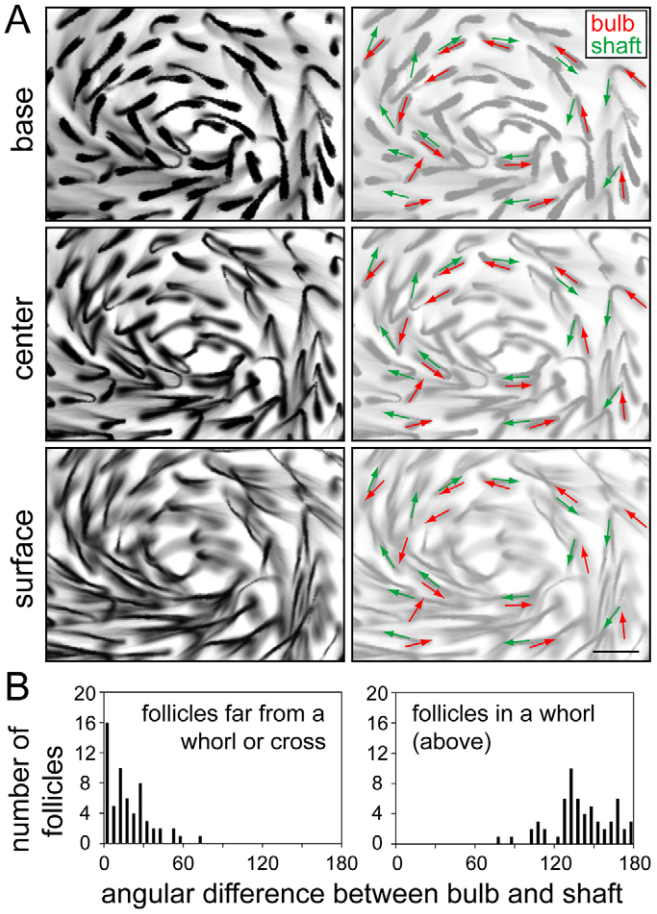

Fig. 4. Bending of hair follicles near the center of a whorl. The whorl is from the back of the P8 *Fz6*$^{-/-}$*;Vangl2*$^{Lp/+}$ mouse skin shown in Fig. 6. (**A**) The center of the whorl is shown at three focal planes: the plane deepest within the dermis (base) shows the follicle bulbs and the plane at the epidermal surface (surface) shows the shafts as they emerge from the skin. The same three panels are reproduced on the right with the vectors for bulb (red) and shaft (green) orientations shown for 14 follicles. (**B**) Histograms showing bulb versus shaft angle differences for follicles from the whorl shown in A (right), and from a region of the same skin located far from a whorl or cross (left). Scale bar: 100 μm.

As expected, the vector map of a WT mouse at P5 shows a nearly parallel arrangement of follicles oriented from nose to tail (Fig. 5, upper left). Small deviations from this pattern occur around the ears and in the center of the head, where follicles at the anterior diverge from the midline and follicles at the posterior converge towards the midline. Despite their interindividual diversity, different *Fz6*$^{-/-}$ (and *Fz6*$^{-/-}$*;Vangl2*$^{Lp/+}$) vector maps at P6, P7 and P8 exhibit a number of common attributes (Figs 5 and 6). First, near the midline, territories of vectors spanning ~20% of the anterior-posterior (A-P) body length are arranged in alternating patterns, such that territories characterized by A-to-P vector orientations alternate with territories characterized by P-to-A vector orientations. Careful inspection of the individual vector maps in Fig. 5 reveals that both P7 skins have five such territories; arrows to the left of the P7 vector maps show the polarities and A-P locations of these territories. Second, points of extreme discontinuity in follicle orientation – referred to hereafter as 'singularities' – show limited variety, as described below.

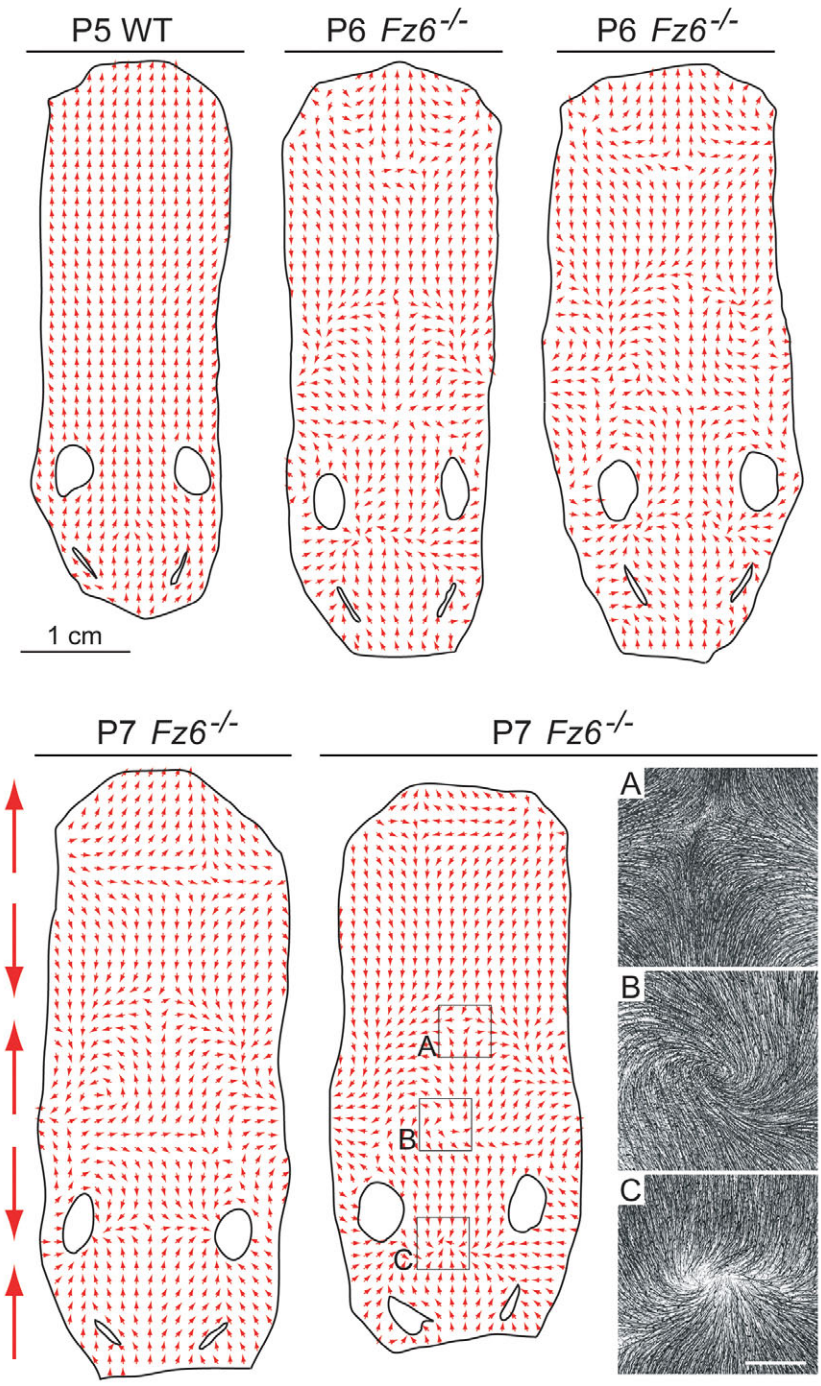

Fig. 5. Global patterns of follicle orientation in WT and *Fz6*$^{-/-}$ mouse back skin at P5-P7. Vector maps were constructed by sampling average follicle orientations at each point on the vector grid. For each skin, anterior is at the bottom. The two narrow openings mark the locations of the eyes, and the two round openings mark the locations of the ears. Images are shown for three singularities (A-C), corresponding to the boxed regions in the adjacent vector map. For the two P7 vector maps, the large arrows to the left represent the anterior-posterior locations and alternating polarities of the five territories of roughly parallel follicles. Scale bar: 2 μm.

Singularities: crosses and whorls

Where two territories with opposing follicle orientations meet, the follicles from both territories progressively reorient so that follicles at the border are aligned similarly but are roughly perpendicular to those within the center of each territory, thereby eliminating sharp discontinuities in the vector field (Fig. 6A). In many cases, this pattern proceeds in one direction over part of the border and then in the reverse direction over the remainder of the border (Fig. 5A; Fig. 6A,F-I). The result is a singularity in the form of a cross.

The second general class of singularity arises from a radially converging or diverging vector field. If there is also a circumferential component, then the singularity develops as a whorl (Fig. 5B and Fig. 6B-E). If the circumferential component is minimal, then the singularity will look like the example shown in Fig. 5C.

By P8, *Fz6*$^{-/-}$ hair patterning appears to be 'complete' in the sense that follicle angles closely conformed to the surrounding pattern, with little evidence of the uncorrelated orientations present 1 week earlier. At this age, the spatial scale of the precisely ordered vector field extended from less than 100 μm to greater than 1 cm (Fig. 6).

Progressive loss of singularities in *Fz6*$^{-/-}$ skin

Computer modeling of the follicle refinement process in *Fz6*$^{-/-}$ mice has predicted a 'competition' between adjacent regions, with the progressive incorporation of less organized vector fields into

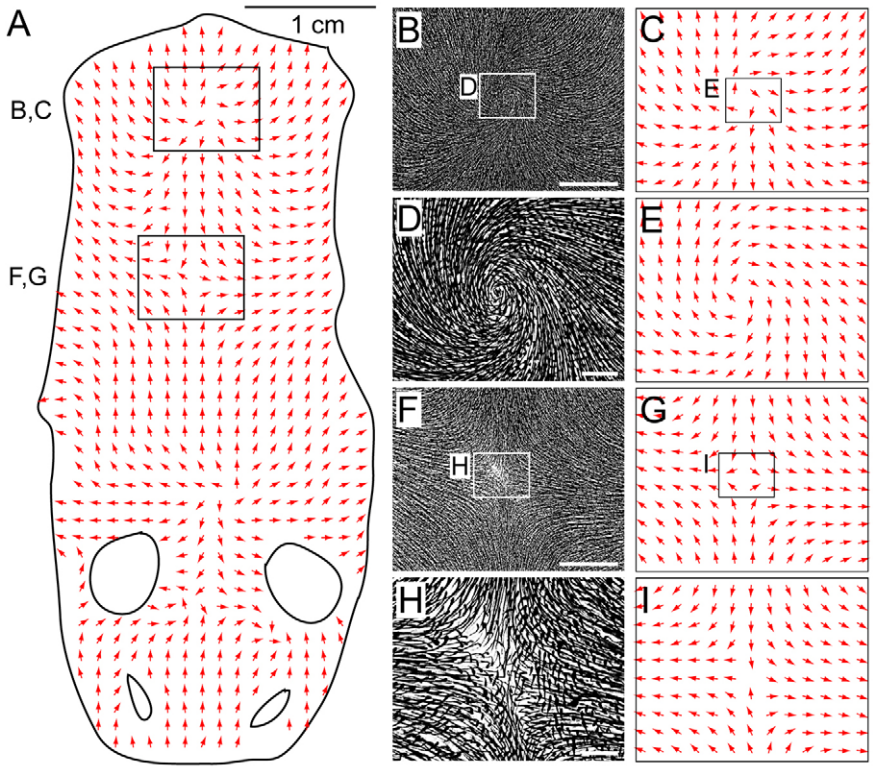

Fig. 6. Short- and long-range order in a *Fz6*$^{-/-}$;*Vangl2*$^{Lp/+}$ mouse skin at P8. (**A**) Vector map showing four singularities spaced at ~1-cm intervals along the midline. (**B-I**) For the two singularities boxed in A, the corresponding images (B,F) and vector maps (C,G) are shown, together with higher magnifications of regions thereof (D,H and E,I). Scale bars: 2 mm in B,F; 300 μm in D,H.

the patterns embodied in better-organized fields (Wang et al., 2006a). To test this prediction, we measured the number of distinct pattern elements by counting the singularities (crosses and whorls) in a set of ten *Fz6*$^{-/-}$ skins between P5 and P8 (Fig. 7). In keeping with the prediction of the model, the number of singularities declined progressively, at a rate of about two per day (Fig. 7). By the method of least squares, the straight line of best fit to the data plotted in Fig. 7 yields a slope of –1.90 singularities per day, with a *P*-value of 0.0075 relative to the null hypothesis of zero slope. The 95% confidence interval places the slope between –0.67 and –3.14.

DISCUSSION

The observations and analyses described here define the time course of local hair follicle refinement and the resulting evolution of the montage of competing patterns in *Fz6*$^{-/-}$ mice. The long range and high precision of *Fz6*$^{-/-}$ follicle patterns are remarkable given how rapidly they develop: at P2, the follicles on the back exhibit little or no local order, whereas 5 days later they have organized into a complex pattern with nearly crystalline precision. This reorganization is all the more striking because it involves the movement of thousands of large multicellular structures.

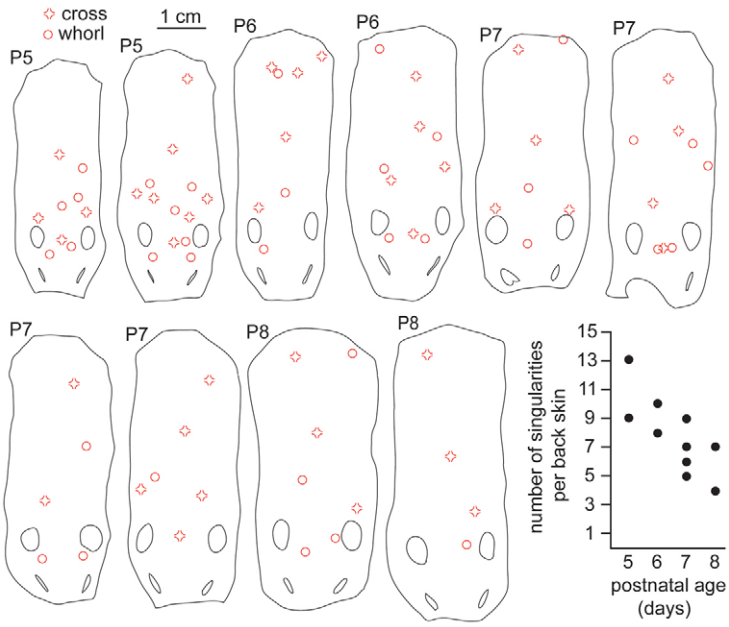

Fig. 7. Progressive decrease in the number of singularities with age in *Fz6*$^{-/-}$ mouse back skin. The locations of singularities (crosses and whorls) are shown for ten back skins. The number of singularities per back skin is plotted as a function of age.

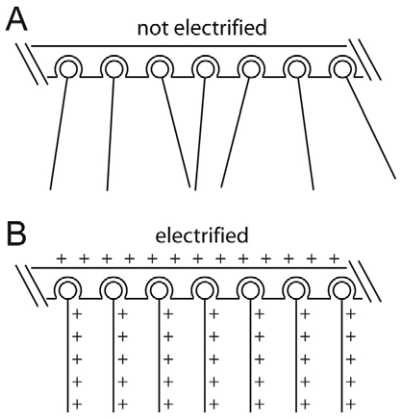

Fig. 8. Physical model of mutual repulsion as a follicle alignment mechanism. Electrically conducting (e.g. copper) rods are suspended from a conducting plate by ball-and-socket joints; the figure shows only one row from the two-dimensional array. (**A**) In the initial configuration, the rods are randomly oriented. (**B**) Electrifying the system aligns the rods because this configuration minimizes electrostatic repulsion between neighbors.

Relationship to the local alignment of insect surface structures

The follicle reorientation phenomena described here bear a striking resemblance to the local reorientation of bristles in insects following surgical manipulations of the cuticle (Locke et al., 1959; Lawrence, 1966). They also resemble, in their final appearance, the globally misaligned, but locally aligned, wing and thoracic hairs seen in typical PCP mutants in *Drosophila*. The dichotomy between the local alignment and the global misalignment that produce whorl or whorl-like patterns led Wong and Adler (Wong and Adler, 1993) to explicitly suggest the existence of distinct local and global orienting systems. Candidate components of the local system in *Drosophila* include the septate junction proteins Gliotactin and Coracle (Venema et al., 2004). Mutations in the corresponding genes (*Gli* and *cora*) disrupt wing hair alignment in a manner that is independent of, and additive with, the patterning defects caused by *fz* mutations. Moreover, the types of hair misorientations seen in *Gli* and *cora* mutants are distinct from those seen in PCP mutants in that local parallelism is disrupted in *Gli* and *cora* mutants with little or no mispatterning on a larger scale. The *Celsr1*$^{-/-}$ and *Fz6*$^{-/-}$ hair follicle phenotypes conform to the general hypothesis set out by Wong and Adler, in that mutation of either gene impairs only the early-acting global orientation system but does not affect the later-acting local alignment system (Guo et al., 2004; Wang et al., 2006a; Ravni et al., 2009). How the further division of the global (i.e. PCP) mechanism into separate *stan*/*fz*/*Vang* and *ds*/*ft* pathways relates to the global/local dichotomy is not clear.

The local refinement program for hair follicles

At present the cell biological basis of local hair follicle alignment is unknown. A critical constraint for any alignment mechanism is the absence of direct contact between follicles: each follicle is separated from its neighbors by an intervening layer of dermis.

As one approach to evaluating potential mechanisms of follicle alignment, it might be useful to consider analogous physical systems. For example, one could model the alignment process with a two-dimensional array of rods joined by ball-and socket joints to the underside of a horizontal plate (Fig. 8A; only one dimension is shown here). To model the *Fz6*$^{-/-}$ phenotype, we suppose that the initial orientation of each rod is randomized, and we then ask whether there is a physical method for aligning the rods. One method, which requires that the entire system be electrically conducting, simply involves electrifying the apparatus (Fig. 8B). If we ignore effects at the edges of the array, then it follows by symmetry that mutual repulsion among the rods produces a minimum energy state in which all rods are perpendicular to the horizontal plate. A more sophisticated version of this model could incorporate the constraint that hair follicles are not generally oriented at right angles to the epidermis. In this case, the angle between each rod and the horizontal plate would be fixed, permitting only free rotation about an axis perpendicular to the plate.

The physical model described above suggests that the realignment mechanism might be based on repulsion between neighboring follicles. Such a mechanism would be inherently local and would promote follicle alignment at all locations within the global pattern. How might mutual repulsion among spatially separated follicles occur? One class of possible mechanisms – by analogy to the mechanism that produces the regularly spaced arrays of hair follicle buds within the epidermis (Sick et al., 2006) – would rely on the production by each follicle of a chemical concentration gradient that repels its neighbors. The principal challenges with such a scenario are to devise a mechanism that (1) allows each follicle to sense the repellent produced by its neighbors without desensitization from its own repellant, and (2) moves each follicle in a directional manner, i.e. away from the repellent. A completely different biological mechanism that also embodies the repulsion concept consists of a process by which each follicle organizes the surrounding dermal cells and/or extracellular matrix so that the effective diameter of the follicle (i.e. its zone of exclusion for neighboring follicles) increases with time.

Models involving attraction rather than repulsion are also possible. For example, if the space between follicles is uniformly filled with a diffusible chemoattractant that is inactivated or taken up when it encounters a follicle, then each follicle will tend to reorient toward the highest concentration of the attractant, which will correspond to the direction of the interfollicular region furthest from a neighboring follicle. The resulting reorienting movements will lead to more uniform interfollicle distances along the length of the follicle shafts, which is the same outcome predicted for the mutual repulsion model.

Regardless of whether or not the particular biological mechanisms described above correspond to that actually used in vivo, the ‘alignment by follicle repulsion’ and ‘alignment by interfollicle chemoattractant’ models might represent useful frameworks for investigating the process of follicle reorientation and pattern formation.

Singularities and the role of competition among large-scale patterns

A progressive expansion of more organized patterns into territories occupied by less organized patterns is one of the central predictions of the local consensus model for follicle alignment described by Wang et al. (Wang et al., 2006a). One obvious consequence of this competition is a decline in the number of pattern elements over time, a phenomenon confirmed here for *Fz6*$^{-/-}$ follicle patterns during the first postnatal week. A less obvious consequence is the stabilization of a small number of singularities – either whorls or crosses – that mark

points where the vector fields of adjacent and highly organized patterns meet but cannot be made locally smooth. Singularities similar to the ones observed in *Fz6*$^{-/-}$ hair patterns are a normal feature of hair patterning in many mammals. For example, whorls are present on the human scalp, between the eyes of horses and cattle, and on the chest adjacent to the front legs in many mammals (Guo et al., 2004).

In the physical sciences, large-scale spatial patterns that evolve under the influence of local forces have been studied in a variety of fields, including hydrodynamics, galactic astrophysics and meteorology (Ball, 1999). They have also been studied computationally, especially in the context of cellular automata (Wolfram, 2002). In considering the mechanisms that produce biological patterns of the type described here, it might be useful to explore the origins and stabilities of analogous patterns in physical systems.

Acknowledgements
We thank Ms Laura Castro for assistance with Fig. 5, Amir Rattner and Hugh Cahill for helpful suggestions, and three anonymous referees for insightful comments on the manuscript. Supported by the Howard Hughes Medical Institute. Deposited in PMC for release after 6 months.

Competing interests statement
The authors declare no competing financial interests.

Supplementary material
Supplementary material for this article is available at
http://dev.biologists.org/lookup/suppl/doi:10.1242/dev.057455/-/DC1

References
Axelrod, J. D. (2009). Progress and challenges in understanding planar cell polarity signaling. *Semin. Cell Dev. Biol.* **20**, 964-971.
Ball, P. (1999). *The Self-Made Tapestry: Pattern Formation in Nature*. Oxford: Oxford University Press.
Curtin, J. A., Quint, E., Tsipouri, V., Arkell, R. M., Cattanach, B., Copp, A. J., Henderson, D. J., Spurr, N., Stanier, P., Fisher, E. M. et al. (2003). Mutation of Celsr1 disrupts planar polarity of inner ear hair cells and causes severe neural tube defects in the mouse. *Curr. Biol.* **13**, 1129-1133.
Devenport, D. and Fuchs, E. (2008). Planar polarization in embryonic epidermis orchestrates global asymmetric morphogenesis of hair follicles. *Nat. Cell Biol.* **10**, 1257-1268.
Guo, N., Hawkins, C. and Nathans, J. (2004). Frizzled6 controls hair patterning in mice. *Proc. Natl. Acad. Sci. USA* **101**, 9277-9281.
Kibar, Z., Vogan, K. J., Groulx, N., Justice, M. J., Underhill, D. A. and Gros, P. (2001). Ltap, a mammalian homolog of Drosophila Strabismus/Van Gogh, is altered in the mouse neural tube mutant Loop-tail. *Nat. Genet.* **28**, 251-255.
Lawrence, P. A. (1966). Gradients in the insect segment: the orientation of hairs in the milkweed bug Oncopeltus fasciatus. *J. Exp. Biol.* **44**, 607-620.
Lawrence, P. A., Struhl, G. and Casal, J. (2007). Planar cell polarity: one or two pathways? *Nat. Rev. Genet.* **8**, 555-563.
Locke, M. (1959). The cuticular pattern in an insect Rhodnius prolixus Stal. *J. Exp. Biol.* **36**, 459-477.
Lyuksyutova, A. I., Lu, C. C., Milanesio, N., King, L. A., Guo, N., Wang, Y., Nathans, J., Tessier-Lavigne, M. and Zou, Y. (2003). Anterior-posterior guidance of commissural axons by Wnt-frizzled signaling. *Science* **302**, 1984-1988.
Montcouquiol, M., Rachel, R. A., Lanford, P. J., Copeland, N. G., Jenkins, N. A. and Kelley, M. W. (2003). Identification of Vangl2 and Scrb1 as planar polarity genes in mammals. *Nature* **423**, 173-177.
Murdoch, J. N., Doudney, K., Paternotte, C., Copp, A. J. and Stanier, P. (2001). Severe neural tube defects in the loop-tail mouse result from mutation of Lpp1, a novel gene involved in floor plate specification. *Hum. Mol. Genet.* **10**, 2593-2601.
Qu, Y., Glasco, D. M., Zhou, L., Sawant, A., Ravni, A., Fritzsch, B., Damrau, C., Murdoch, J. N., Evans, S., Pfaff, S. L. et al. (2010). Atypical cadherins Celsr1-3 differentially regulate migration of facial branchiomotor neurons in mice. *J. Neurosci.* **30**, 9392-9401.
Ravni, A., Qu, Y., Goffinet, A. M. and Tissir, F. (2009). Planar cell polarity cadherin Celsr1 regulates skin hair patterning in the mouse. *J. Invest. Dermatol.* **129**, 2507-2509.
Saburi, S., Hester, I., Fischer, E., Pontoglio, M., Eremina, V., Gessler, M., Quaggin, S. E., Harrison, R., Mount, R. and McNeill, H. (2008). Loss of Fat4 disrupts PCP signaling and oriented cell division and leads to cystic kidney disease. *Nat. Genet.* **40**, 1010-1015.
Sick, S., Reinker, S., Timmer, J. and Schlake, T. (2006). WNT and DKK determine hair follicle spacing through a reaction-diffusion mechanism. *Science* **314**, 1447-1450.
Simons, M. and Mlodzik, M. (2008). Planar cell polarity signaling: from fly development to human disease. *Annu. Rev. Genet.* **42**, 517-540.
Song, H., Hu, J., Chen, W., Elliott, G., Andre, P., Gao, B. and Yang, Y. (2010). Planar cell polarity breaks bilateral symmetry by controlling ciliary positioning. *Nature* **466**, 378-382.
Tissir, F., Bar, I., Jossin, Y. and Goffinet, A. M. (2005). Protocadherin Celsr3 is crucial in axonal tract development. *Nat. Neurosci.* **8**, 451-457.
Tissir, F., Qu, Y., Montcouquiol, M., Zhou, L., Komatsu, K., Shi, D., Fujimori, T., Labeau, J., Tyteca, D., Courtoy, P. et al. (2010). Lack of cadherins Celsr2 and Celsr3 impairs ependymal ciliogenesis, leading to fatal hydrocephalus. *Nat. Neurosci.* **13**, 700-707.
Venema, D. R., Zeev-Ben-Mordehai, T. and Auld, V. J. (2004). Transient apical polarization of Gliotactin and Coracle is required for parallel alignment of wing hairs in Drosophila. *Dev. Biol.* **275**, 301-314.
Wang, Y., Thekdi, N., Smallwood, P. M., Macke, J. P. and Nathans, J. (2002). Frizzled-3 is required for the development of major fiber tracts in the rostral CNS. *J. Neurosci.* **22**, 8563-8573.
Wang, Y., Badea, T. and Nathans, J. (2006a). Order from disorder: self-organization in mammalian hair patterning. *Proc. Natl. Acad. Sci. USA* **103**, 19800-19805.
Wang, Y., Guo, N. and Nathans, J. (2006b). The role of Frizzled3 and Frizzled6 in neural tube closure and in the planar polarity of inner ear sensory hair cells. *J. Neurosci.* **26**, 2147-2156.
Wang, Y., Zhang, J., Mori, S. and Nathans, J. (2006c). Axonal growth and guidance defects in Frizzled3 knock-out mice: a comparison of diffusion tensor magnetic resonance imaging, neurofilament staining, and genetically directed cell labeling. *J. Neurosci.* **26**, 355-364.
Wolfram, S. (2002). *A New Kind of Science*. Champagne, IL: Wolfram Media.
Wong, L. L. and Adler, P. N. (1993). Tissue polarity genes of Drosophila regulate the subcellular location of prehair initiation in pupal wing cells. *J. Cell Biol.* **123**, 209-221.
Wigglesworth, V. B. (1940). Local and general factors in the development of 'pattern' in Rhodnius prolixus. *J. Exp. Biol.* **17**, 180-200.
Zhou, L., Bar, I., Achouri, Y., Campbell, K., De Backer, O., Hebert, J. M., Jones, K., Kessaris, N., de Rouvroit, C. L., O'Leary, D. et al. (2008). Early forebrain wiring: genetic dissection using conditional Celsr3 mutant mice. *Science* **320**, 946-949.